SI - Impact of binder content on particle fracture and microstructure of solvent-free electrodes for Li-ion batteries

Guillaume Matthews*[a,d], Benjamin Meyer[a,d], Christopher Doerrer[b], Julia Ramírez-González[a], Ed Darnbrough[a,d], Noël Hallemans[c,d], David Armstrong[a,d], Patrick S. Grant[a,d]

[a]Department of Materials, University of Oxford, Parks Road, OX1 3PH, Oxford, UK

[b]Department of Mechanical and Industrial Engineering, University of Toronto, Canada

[c]Department of Engineering Science, University of Oxford, Parks Road, OX1 3PJ, Oxford, UK

[d]The Faraday Institution, Quad One, Harwell Science and Innovation Campus, Didcot, UK

*E-mail: guillaume.matthews@materials.ox.ac.uk

Materials and methods

Electrochemical characterisation

Impedance measurements were taken at room temperature using a Biologic VSP potentiostat (measurement accuracy ±0.1%), over the frequency range 1 mHz – 10 kHz with 10 frequencies per decade and a nominal AC voltage amplitude of 10 mV. Every EIS measurement was performed after a relaxation period of 2 h to allow the electrode to reach steady-state. The conditions of linearity and stationarity of the EIS data [1] were further assessed using measurement model software [2]. The EIS measurement of the 4 wt.% electrode at 100% SOC showed poor compliance with the measurement model at frequencies higher than 1222 Hz. Therefore, only impedance data at frequencies lower than 1222 Hz were used for the subsequent analysis.

The equivalent circuit model of Fig. 5 was used to model the measured EIS data. The high frequency semi-circle, modelled by a RC-pair, showed no SOC dependence and can, hence, be attributed to a contact resistance. The mid-frequency semi-circle shows a typical charge transfer SOC dependence and is, hence, attributed to those kinetics. Due to the roughness of particles, a constant-phase element (CPE) $Z_{\mathrm{CPE}}(\omega)$:

$$Z_{\mathrm{CPE}}(\omega) = \frac{1}{\mathrm{CPE}(j\omega)^{\alpha}} \qquad \alpha \in [0,1] \tag{1}$$

was used for the fitting instead of a capacitor. The low frequency semi-circle did not depend significantly on SOC and could, hence, be attributed to electrolyte diffusion. At very low

frequencies, solid state diffusion could be resolved, which can be modelled by a Warburg element for Fickian diffusion in spherical particles $Z_{\mathrm{W}}(\omega)$ [3]:

$$Z_{\mathrm{W}}(\omega) = R_{\mathrm{w}} \frac{\tanh\sqrt{j\omega\tau}}{\sqrt{j\omega\tau} - \tanh\sqrt{j\omega\tau}}. \tag{2}$$

with R_{w} the solid-sate diffusion resistance. The solid state diffusion time-scale τ was only identifiable at low enough frequency when approximated to a vertical line. This was only the case for the 0.5 wt.% binder sample at 70, 80, 90, and 100 % SOC.

Parameter fitting was performed in MATLAB using particle swarm optimisation. The impedance fit in Fig. 5D for the 4 wt.% binder electrode (purple) is shown in the frequency range [10 kHz, 1 mHz], while the measured impedance data is only shown in the range [1222 Hz, 1 mHz] (which was the data used for fitting).

Additional figures

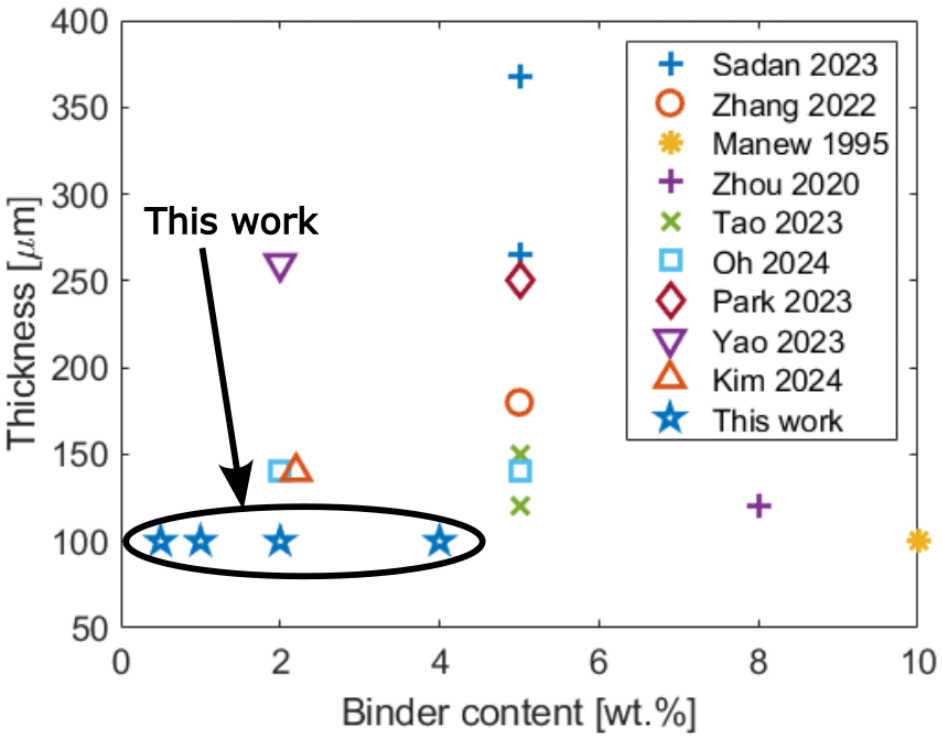

Figure 1: Summary of the current research on solvent-free electrodes in terms of the typical electrode thickness and binder fractions investigated. [4]–[12].

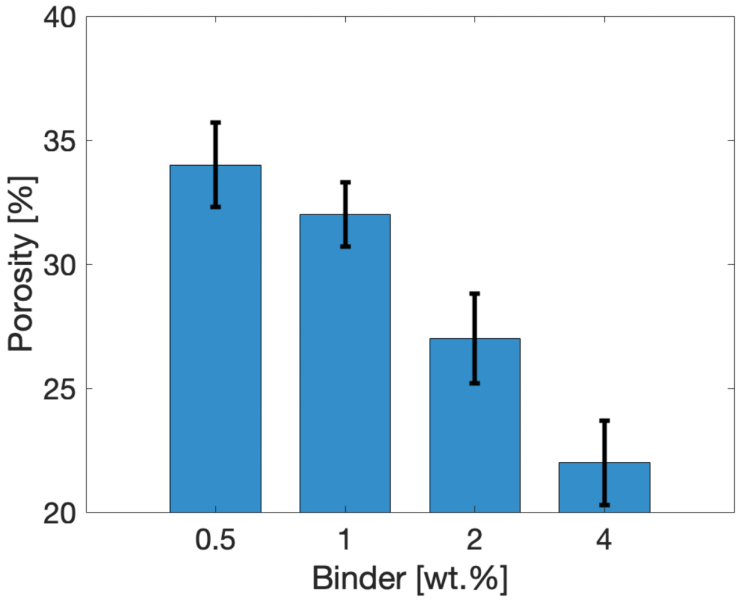

Figure 2: The porosity of 14 mm disks cut from of 0.5, 1, 2 and 4 wt.% PTFE electrodes calendered to 100 μm thickness.

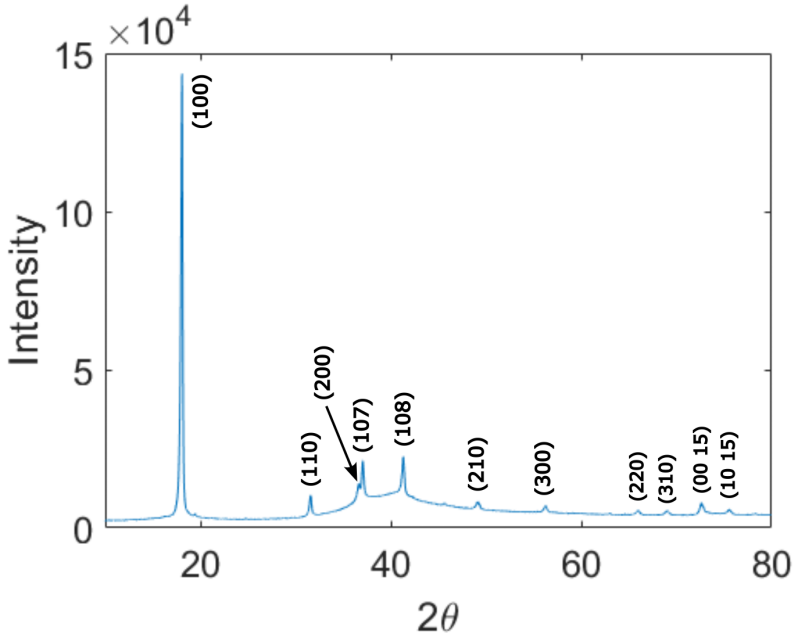

Figure 3: XRD pattern of the feedstock PTFE powder.

Index	(100)	(110)	(200)	(107)	(108)	(210)	(300)	(220)	(310)	(00 15)	(10 15)
Angle [2θ]	18.1	31.6	36.6	37.1	41.3	49.1	56.3	66.0	69.0	72.6	75.6
Spacing [Å]	4.90	2.83	2.45	2.43	2.18	1.85	1.63	1.42	1.36	1.30	1.26

Table 1: Individual peak characteristics extracted from the XRD pattern in Fig. 3.

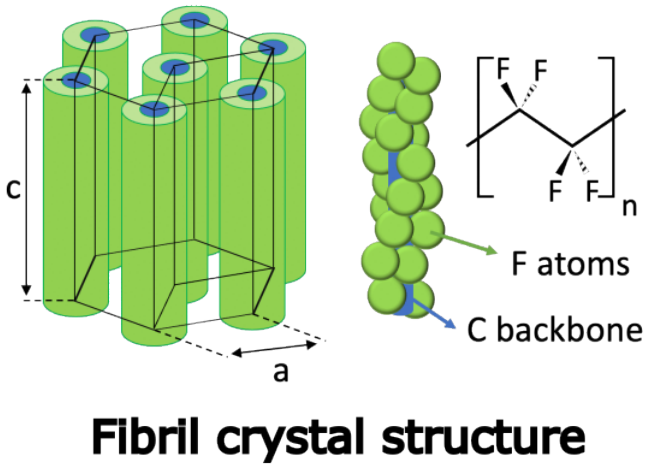

Figure 4: Pseudo-hexagonal crystal structure of PTFE, redrawn from [13].

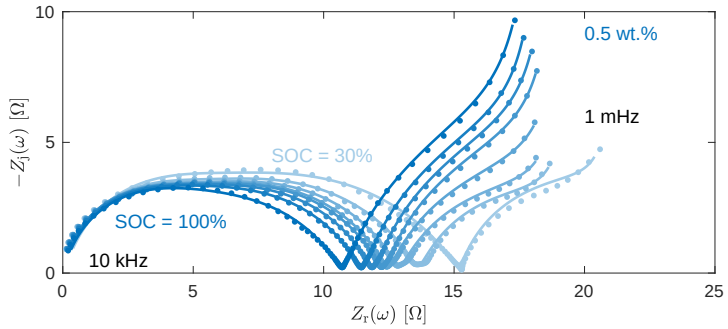

Figure 5: Nyquist plot of the impedance of the 0.5 wt.% electrode for SOCs from 30% up to 100%, used for system identification.

SOC [%]	30	40	50	60	70	80	90	100
R_{contact} [Ω]	3.5	3.5	3.6	3.6	3.6	3.5	3.3	3.1
C_{contact} [F]	3.8e-5	3.2e-5	2.9e-5	2.8e-5	2.8e-5	2.9e-5	3.1e-5	3.6e-5
R_{ct} [Ω]	12	10	9.3	8.8	8.6	8.3	8.1	7.5
CPE_{ct} [s^{α}/Ω]	10e-4	7.6e-4	6.5e-4	5.9e-4	5.7e-4	5.5e-4	5.6e-4	6.6e-4
α_{ct}	0.66	0.71	0.73	0.75	0.75	0.75	0.74	0.72
R_{el} [Ω]	5.6	5.3	5.9	6.2	5.9	6.0	6.2	6.7
CPE_{el} [s^{α}/Ω]	6.1	4.6	4.2	5.1	6.8	6.9	6.7	6.2
α_{el}	0.90	0.82	0.79	0.83	0.90	0.91	0.92	0.91
R_{w} [Ω]	2.3	3.7	3.7	4.7	5.7	5.6	5.2	5.8
τ [s]	390	700	700	620	480	420	360	380

Table 2: Best-fit parameters from the equivalent circuit analysis for the NMC-based electrode containing 0.5 wt.% binder in a half-cell configuration and three electrode set-up with a reference Li electrode. The corresponding impedance data and fits are shown in Fig. 5

Binder content [wt.%]	0.5	4
R_{contact} [Ω]	3.1	30
C_{contact} [F]	3.6e-5	1.7e-5
R_{ct} [Ω]	7.5	6.4
CPE_{ct} [s^{α}/Ω]	6.6e-4	9.5e-4
α_{ct}	0.72	0.88
R_{el} [Ω]	6.7	21
CPE_{el} [s^{α}/Ω]	6.2	2.1
α_{el}	0.91	0.71
R_{w} [Ω]	5.8	4.7
τ [s]	380	500

Table 3: Best-fit parameters obtained from the equivalent circuit analysis for the NMC-based electrodes containing 0.5 wt.% and 4 wt.% binder in a half-cell configuration and three electrode set-up with a reference Li electrode at 100% SOC.

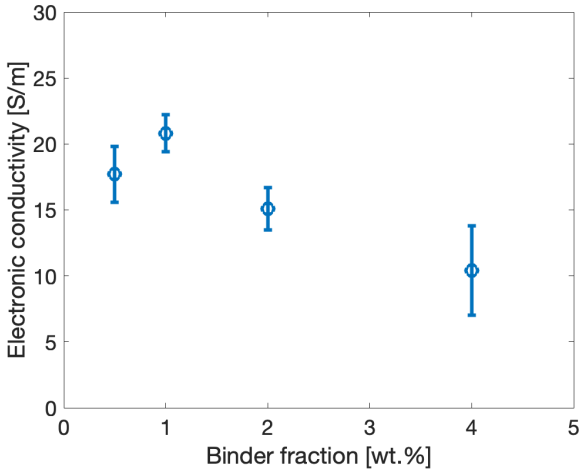

Figure 6: Electronic conductivity of solvent-free electrodes containing 0.5, 1, 2 and 4 wt.% PTFE.

Electrode characteristics

Binder [wt.%]	C-additive [wt.%]	Thickness [μm]	Areal loading [mAh/cm^2]
0.5	3.5	102	29.5
0.5	3.5	104	29.4
1	3.5	107	29.8
1	3.5	105	30.5
2	3.5	107	31.1
2	3.5	106	32.3
4	3.5	108	33.4
4	3.5	111	33.4

Table 4: Characteristics of the electrodes used in half-cells.

References

[1] S. Wang, J. Zhang, O. Gharbi, V. Vivier, M. Gao, and M. E. Orazem, "Electrochemical impedance spectroscopy," *Nature Reviews Methods Primers*, vol. 1, no. 1, p. 41, 2021.

[2] M. E. Orazem, "Measurement model for analysis of electrochemical impedance data," *Journal of Solid State Electrochemistry*, vol. 28, no. 3, pp. 1273–1289, 2024.

[3] A. M. Bizeray, J.-H. Kim, S. R. Duncan, and D. A. Howey, "Identifiability and parameter estimation of the single particle lithium-ion battery model," *IEEE Transactions on Control Systems Technology*, vol. 27, no. 5, pp. 1862–1877, 2018.

[4] M. K. Sadan, G. J. Lian, R. M. Smith, and D. Cumming, "Co, ni-free ultrathick free-standing dry electrodes for sustainable lithium-ion batteries," *ACS Applied Energy Materials*, vol. 6, pp. 12 166–12 171, 24 Dec. 2023, ISSN: 25740962. DOI: 10.1021/acsaem.3c02448.

[5] Y. Zhang, F. Huld, S. Lu, C. Jektvik, F. Lou, and Z. Yu, "Revisiting polytetrafluorethylene binder for solvent-free lithium-ion battery anode fabrication," *Batteries*, vol. 8, 6 Jun. 2022, ISSN: 23130105. DOI: 10.3390/batteries8060057.

[6] V Manev, I Naidenov, B Puresheva, P Zlatilova, and G Pistoia, *Electrochemical performance of natural brazilian graphite as anode material for lithium-ion rechargeable cells*, 1995.

[7] H. Zhou, M. Liu, H. Gao, *et al.*, "Dense integration of solvent-free electrodes for li-ion supercabattery with boosted low temperature performance," *Journal of Power Sources*, vol. 473, Oct. 2020, ISSN: 03787753. DOI: 10.1016/j.jpowsour.2020.228553.

[8] R. Tao, B. Steinhoff, X. G. Sun, *et al.*, "High-throughput and high-performance lithium-ion batteries via dry processing," *Chemical Engineering Journal*, vol. 471, Sep. 2023, ISSN: 13858947. DOI: 10.1016/j.cej.2023.144300.

[9] H. Oh, G. S. Kim, B. U. Hwang, J. Bang, J. Kim, and K. M. Jeong, "Development of a feasible and scalable manufacturing method for ptfe-based solvent-free lithium-ion battery electrodes," *Chemical Engineering Journal*, vol. 491, Jul. 2024, ISSN: 13858947. DOI: 10.1016/j.cej.2024.151957.

[10] G. Park, H. S. Kim, and K. J. Lee, "Solvent-free processed cathode slurry with carbon nanotube conductors for li-ion batteries," *Nanomaterials*, vol. 13, 2 Jan. 2023, ISSN: 20794991. DOI: 10.3390/nano13020324.

[11] W. Yao, M. Chouchane, W. Li, *et al.*, "A 5 v-class cobalt-free battery cathode with high loading enabled by dry coating," *Energy and Environmental Science*, vol. 16, pp. 1620–1630, 4 Feb. 2023, ISSN: 17545706. DOI: 10.1039/d2ee03840d.

[12] J. Kim, K. Park, M. Kim, *et al.*, "10 mah cm-2 cathode by roll-to-roll process for low cost and high energy density li-ion batteries," *Advanced Energy Materials*, vol. 14, 10 Mar. 2024, ISSN: 16146840. DOI: 10.1002/aenm.202303455.

[13] K. Sato, Y. Tominaga, Y. Imai, T. Yoshiyama, and Y. Aburatani, "Deformation capability of poly(tetrafluoroethylene) materials: Estimation with x-ray diffraction measurements," *Polymer Testing*, vol. 113, Sep. 2022, ISSN: 01429418. DOI: 10.1016/j.polymertesting.2022.107690.